

2



Lawrence Berkeley Laboratory

UNIVERSITY OF CALIFORNIA

Materials & Chemical
Sciences Division

RECEIVED
LAWRENCE
BERKELEY LABORATORY

FEB 19 1988

National Center for Electron Microscopy

LIBRARY AND
DOCUMENTS SECTION

Submitted to Nature

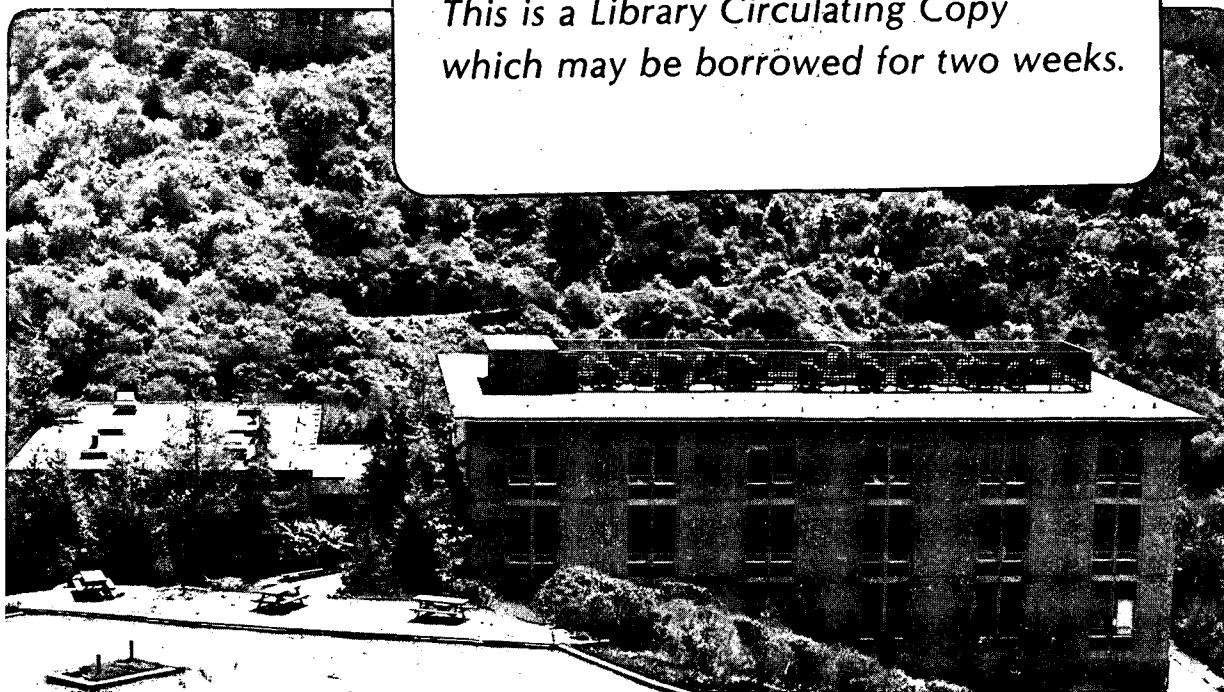
On the Structure of $(\text{CuO})_2$ Double Layers in
Superconducting $\text{YBa}_2\text{Cu}_3\text{O}_7$

H.W. Zandbergen, R. Gronsky, K. Wang, and G. Thomas

January 1987

TWO-WEEK LOAN COPY

*This is a Library Circulating Copy
which may be borrowed for two weeks.*



LBL-24671

2

DISCLAIMER

This document was prepared as an account of work sponsored by the United States Government. While this document is believed to contain correct information, neither the United States Government nor any agency thereof, nor the Regents of the University of California, nor any of their employees, makes any warranty, express or implied, or assumes any legal responsibility for the accuracy, completeness, or usefulness of any information, apparatus, product, or process disclosed, or represents that its use would not infringe privately owned rights. Reference herein to any specific commercial product, process, or service by its trade name, trademark, manufacturer, or otherwise, does not necessarily constitute or imply its endorsement, recommendation, or favoring by the United States Government or any agency thereof, or the Regents of the University of California. The views and opinions of authors expressed herein do not necessarily state or reflect those of the United States Government or any agency thereof or the Regents of the University of California.

On the Structure of $(\text{CuO})_2$ Double Layers in Superconducting $\text{YBa}_2\text{Cu}_3\text{O}_7$

H.W. Zandbergen, R. Gronsky, K. Wang and G. Thomas

National Center for Electron Microscopy

Materials and Chemical Sciences Division, Lawrence Berkeley Laboratory, University of California, Berkeley,
California 94720

Abstract

Based upon a high resolution electron microscopy analysis of planar defects in superconducting $\text{YBa}_2\text{Cu}_3\text{O}_7$, the identity of a CuO double layer intercalation has been revealed. Within this double layer, the Cu atoms remain in planar four-fold coordination with O , identical to their arrangement in the single CuO layers of the $\text{YBa}_2\text{Cu}_3\text{O}_7$ matrix.

Introduction

Since the report that multiphase mixtures with the nominal composition $\text{La}_{2-x}\text{Ba}_x\text{CuO}_{4-y}$ exhibit possible superconductivity [1], research on this class of quaternary oxides has increased enormously. The superconducting compound in the original mixture was rapidly identified as $\text{La}_{1.85}\text{Ba}_{0.15}\text{CuO}_4$ [2], and subsequent research concentrated on the most suitable cation substitutions in this compound. A new oxide with a considerably higher T_c was very soon found in the phase system $\text{Y}_2\text{O}_3 - \text{BaO} - \text{CuO}$ [3], later identified by several groups as $\text{YBa}_2\text{Cu}_3\text{O}_{7-\delta}$ [4], and now commonly known as the 1-2-3 compound. Intensive activity in structural characterization followed. The structure of the "bulk" material has been precisely determined by neutron powder diffraction [5] in agreement with single crystal x-ray diffraction [6], and is shown in Figure 1a. High resolution electron microscopy has been performed by several groups [6-11], all confirming the "bulk" structure, but also reporting the existence of several types of local structural modifications, mostly planar in character.

Ourmazd *et al* [10] report the existence of two extra layers (one Y layer and one CuO layer) inserted at the position of the CuO layer ($z=0$). Viegers *et al* [12] report defects at the grain boundary having a lattice parameter of 1.38 nm instead of the 1.16 nm characteristic of the

undeformed structure. Antiphase boundaries with a $c/3$ shift were characterized by Zandbergen *et al* [13] and Domenges *et al* (14). Another type of planar defect was found [13] to exist at the mirror plane locations ($z=0$ or $z=1/2$) in $\text{ErBa}_2\text{Cu}_3\text{O}_7$. The defect, an inclusion of an extra layer leading to a c axis dimension of about 1.36 nm, was shown to be a double Er layer with a stacking order similar to the double LaO layer in $\text{La}_2\text{Sr}_x\text{CuO}_4$ [2]. Furthermore [100] 90° rotation twins, across which the b axis aligns with a c axis, have also been studied [15].

Recently the decomposition of the 1-2-3 phase was observed to nucleate at free surfaces and proceed by the insertion of an extra CuO layer at the location of the original CuO single layer [16]. This insertion leads to an enlargement of the c axis by 15%, due to the presence of $(\text{CuO})_2$ double layers. The decomposition reaction occurs even at room temperature and may be enhanced by moisture. It is emphasized that in freshly-cleaved specimens there is no evidence of planar defects resulting from inserted CuO layers. Consequently many of the early HREM reports on inclusions and stacking defects along the c axis are questionable since, at that time, it was not known that the material decomposed upon contact with air.

The purpose of this research is to clarify the nature of the $(\text{CuO})_2$ double-layer defects in superconducting $\text{YBa}_2\text{Cu}_3\text{O}_7$ by detailed local structure determination employing high resolution electron microscopy and computer-assisted image analysis.

Experimental Procedures

High resolution electron microscopy was carried out in a JEOL JEM 200CX electron microscope operating at 200 kV and equipped with a top entry $\pm 10^\circ$ double-tilt goniometer, and the Berkeley Atomic Resolution Microscope [17] operating at 1000kV and equipped with a $\pm 40^\circ$ biaxial, double-tilt-lift goniometer.

Specimens for high resolution electron microscopy were prepared in a variety of ways. Powdered $\text{YBa}_2\text{Cu}_3\text{O}_7$ was cooled quickly from room temperature to 77K in liquid N_2 , and a few droplets of a suspension of the powder were put onto conventional holey carbon films over Cu grids. In a parallel study, small wedge-shaped fragments (about 0.5 mm long) were selected after cleaving pieces of sintered pellets of $\text{YBa}_2\text{Cu}_3\text{O}_7$. These fragments were mounted in Cu or Au folding grids. Some material was also subjected to ion milling; however, these samples were found to contain a prominent amorphous layer which complicates image interpretation and in addition showed a marked increase in their rate of defect formation. Because this study is sensitive to such defect formation, the ion milling procedure was abandoned.

Image calculations were performed using the CEMPAS[®] simulation software developed at the National Center for Electron Microscopy [18]. Image processing was carried out using

SEMPER[®] software [19] on images digitized via an Eikonix[®] camera.

Experimental Results and Discussion

In Figure 2, two different images of defects are observed, as indicated by the different contrast features within the planar-faulted regions (arrowed). Computer simulation was used to determine whether these images came from two different defects or whether both images came from the same defect in different orientations. The procedure is relatively straightforward, since the surrounding image of the perfect $\text{YBa}_2\text{Cu}_3\text{O}_7$ matrix serves as an internal calibration on specimen thickness and the defocus. Images of this "normal" structure were first simulated using published lattice parameters of $\text{YBa}_2\text{Cu}_3\text{O}_7$ [20]. Matching between experimental and computed images was sought by varying the objective lens defocus between 0 and -140 nm and the specimen thickness between 2 and 20 nm in the calculations. Images of defect structures were then calculated using a computational "unit cell" with a *c* axis 7 times larger than that of the actual 1-2-3 structure. In this model, two defective layers were introduced as shown in Fig.1(b): one with a shift between the CuO planes of $a/2$ (henceforth called the $a/2$ defect) and one with a shift of $b/2$ (the $b/2$ defect). It is noted that depending upon the viewing or projection direction, these defects show either mirror or glide symmetries (see Fig.3). The distance between the two defects was taken to be two standard unit cells apart, a distance observed in one of the HREM images. Calculations were carried out for four different double CuO layers in which the occupancy of the Cu sites was either 1/2 or 1 and oxygen was situated at the normally occupied or normally vacant positions of the lattice, as shown in Figure 4.

In order to quantify the intensity variation in the images, line scans were made across the defects in the averaged experimental images and the calculated images, shown for comparison in figure 4. From these scans it is evident that the intensity of all Cu atoms is identical except for those Cu atoms within the defect layer.

Using the image of the $\text{YBa}_2\text{Cu}_3\text{O}_7$ matrix as a reference, it was found that the best fit between the experimental images and the calculated ones occurred when the calculational model was oriented in a [010] direction. The distinguishing feature in these images is the fact that the intensities of all Cu atom positions are approximately the same; this is to be expected since they all appear in identical mixed columns (Cu and O) along the [010] projection direction. In the orthogonal [100] projection, the Cu atoms at the $z=0$ plane should image with reduced intensity because they are *not* interspersed with oxygen atoms along the projection direction (this is clearly seen in the calculations). Applying the same comparison technique to the defect images, it is seen that the defect showing mirror symmetry fits the model well in a [010] orientation while the defect

showing glide symmetry fits the model better in the wrong, i.e. the orthogonal [100], orientation. This error necessitates a change in the proposed model.

An obvious correction is suggested by the image matching results obtained in this study; namely, the observed contrast always appears to be consistent with double Cu-O-Cu-O... chains along the projected image direction. If the atomic arrangement of the $a/2$ defect is made the same as in the proposed model but with locally reversed a and b axes (a configuration that can be achieved by exchanging oxygen atoms and vacancies in the $z=0$ plane), then the resulting structure will have double Cu-O-Cu-O... chains that are aligned in the direction of the shift (along the a axis). If the displacement that is necessary to accommodate the inclusion of the extra CuO layer occurs along the b axis, then the structure of the YBa₂Cu₃O₇ matrix is retained, again with double Cu-O-Cu-O... chains along the direction of the shift (the b axis). It was this model that was employed in detailed calculations for image matching.

Image simulations were carried out with a slice thickness of 0.382 and 0.389 nm for the [100] and [010] direction, respectively. By this choice of conditions all the atoms in the unit cell are projected onto one plane and any information regarding the position of the atoms within the unit cell along the electron beam direction is ignored. Although this approximates the experimental conditions obtained in high resolution phase contrast imaging, it prohibits any determination from a single image whether the observed glide defect pattern of Cu atoms is due to a shift of $1/2a$ alone, or whether the shift contains an orthogonal component (e.g. $1/2a + \alpha b$, where α may assume any fractional value). Fortunately such information can be obtained by comparing high resolution electron micrographs obtained in different specimen orientations. For the defects imaged here, an obvious direction to compare with the [100] image is the [110] image; together these two projections make it possible to decide clearly whether the contrast observed at the location of the (CuO)₂ double layer is due to a displacement along one axis or two.

Using the high angle tilting capability of the ARM, it was possible to image the same defective regions of a crystal in both [100] and [110] orientations at high resolution. In these experiments, it was observed that in $\langle 110 \rangle$ projections, the images revealed a shift of $0.5d_{(110)}$ at the defect sites. Furthermore mirror and glide defect patterns are observed for both the [100] and [010] orientations. These observations suggest that introduction of the extra CuO layer coincides with a shift of $1/2a$ or $1/2b$ leading to glide and mirror defect features in the images as shown in Figure 2.

From the line scans shown in Figure 4, it is clear that the contrast of the Cu and O atoms in the mirror defect is nearly identical to the contrast at the Y atom position. This unfortunately implies that it is not possible to determine directly from the images whether the black dots in the mirror defect originate from a mixed column of Cu and O atoms or from a column of Y atoms. However, a number of chemical and structural considerations narrow the possibilities.

Direct substitution of Cu and O atoms by Y atoms would necessitate Y having two-fold coordination with oxygen. This follows from the high resolution results; the observed intensity variations are only consistent with isolated Y ions in the double layer, not Y and O, since the mixed atomic column image would lead to different intensity variations. However, two-fold coordination is not an acceptable configuration for Y, since Y requires at least six-fold coordination with oxygen. Furthermore, insertion of a Y atom at the Cu position would increase the *c* axis lattice parameter, due to the larger size of the Y³⁺ ion. Direct measurements of the high resolution images show that the actual increase of the *c* axis due to the insertion of the defect layer is 15.0±0.5%, whereas values of 17% or more are to be expected if Y is included in the defect plane. Moreover the observed 15% increase in the *c*-axis indicates that the Cu-O distance in the defect plane along the *c* axis is about 0.185nm, which is exactly the Cu-O distance along the *c* axis for the YBa₂Cu₃O₇ matrix observed by neutron powder diffraction [20].

The best fit between experimental and calculated images was obtained for the model in which Cu-O-Cu-O... chains occur in the direction of the displacement required to accommodate the extra CuO layer. This means that a shift along the *b* axis will leave the oxygen atoms at their original position, whereas a shift along the *a* axis will lead to a rearrangement of the oxygen atoms in both CuO planes (Fig. 2). In the latter case the oxygen atoms will occupy the originally vacant sites. Only in this way can the planar four-fold coordination of Cu be maintained. This planar four-fold coordination is often observed in Cu compounds (for instance CuO), and is known to be energetically favorable. That it is also a stable coordination in this specific structure can be deduced from the fact that it exists in the "bulk" YBa₂Cu₃O₇ matrix and furthermore, for YBa₂Cu₃O_{7- δ} in the approximate range 0.4< δ <0, a superstructure occurs, marked by a doubling of the *a* axis and an alternating sequence of Cu-O-Cu-O... and Cu-vacancy-Cu-vacancy... chains having four-fold and two-fold coordination of Cu atoms respectively [7].

This study also reveals a helpful feature of phase contrast imaging applied to the oxide superconductors. Because of their very slight differences in image contrast, it is usually very difficult to distinguish whether a YBa₂Cu₃O₇ crystal is in [100] orientation or in [010] orientation, particularly because the rotational symmetry of both directions is the same. Two methods can be used however. First, the *c/a* ratio can be determined. Unfortunately, for YBa₂Cu₃O₇ this is not very reliable because the lattice can expand perpendicular to the *c* axis (see Figure 1) in thin regions. Furthermore, one must be aware that the measured *c/a* ratio will also depend on imperfections in the lenses (of both the electron microscope and the photographic projector) and the position of the image on the negative (deviations generally increase towards the edge of the negative).

Second, comparisons between calculated and observed images can be used. Once more it is unfortunate that the difference between images calculated for the [100] and [010] orientations is

so small, since the structural differences between these directions arise solely from the oxygen/vacancy ordering in the CuO plane. However, as is shown above, it is possible to determine the crystal orientation by distinguishing the contrast due to the presence or absence of oxygen ions at the $z = 0$ plane, provided the crystal is thin enough and the point resolution is such that isolated Cu atoms can be imaged separately (see Fig. 5). Although this is a stringent set of requirements, they do identify conditions under which the [100] or [010] directions of the orthorhombic phase can be distinguished.

The most serious problem in the interpretation of all defects is the presence of local lattice bending in the neighborhood of their core structures as is shown in Fig. 6. When the crystal is very thin (less than approximately 4 nm) and the defect is extended through the entire sample thickness, the best conditions for imaging are obtained. However, if the defect is restricted to the surface or if it jogs over neighboring CuO planes, which will occur often in thicker crystals, the lattice will bend to accommodate the structural changes of the defect. The image obtained from such configurations will show local differences in contrast, very similar to bend contours in thin crystals. Due to such local changes in the lattice orientation, direct interpretation of the image is impossible. Image simulations could in principle be used to determine the structure, but calculations are typically very time-consuming and do not guarantee any single choice of actual structure.

Although there is presently no data available on the effect of the (CuO)₂ double layers on superconducting performance, it would be interesting to note in particular how the critical current varies with the density of such defects, since they cause an increase in the number of superconduction electrons (i.e. those within the CuO planes). A possible problem may be the bifurcation of the conduction planes at the junction between a double layer and the normal single-layer structure, and any determination of the atomic structure of the bifurcation region will also require imaging in more than one orientation.

Conclusions

High resolution electron microscopy has revealed the intercalation behavior of Cu and O in YBa₂Cu₃O₇. This intercalation is only observed along the CuO planes, and leads to the formation of (CuO)₂ double layers by initiation at the surface of the material.

Detailed structure analysis of the intercalation defects is possible because the known structure of the YBa₂Cu₃O₇ matrix enables a precise determination to be made of the adjustable parameters of objective lens defocus and specimen thickness at the time the image was recorded. Accuracy in comparing calculated and experimental images is increased by using line scans that give a plot of contrast level versus position along the *c* axis.

Because the structure of YBa₂Cu₃O₇ is relatively simple, the effect of oxygen on the

structure can be analyzed in a straightforward manner. It is shown that the difference between the [100] and [010] directions of the orthogonal phase is detectable in the images of the oxygen atoms within the $z=0$ plane, but it is only possible to discriminate between these two directions if the performance of the microscope is such that Ba, Y and Cu atoms are individually resolved.

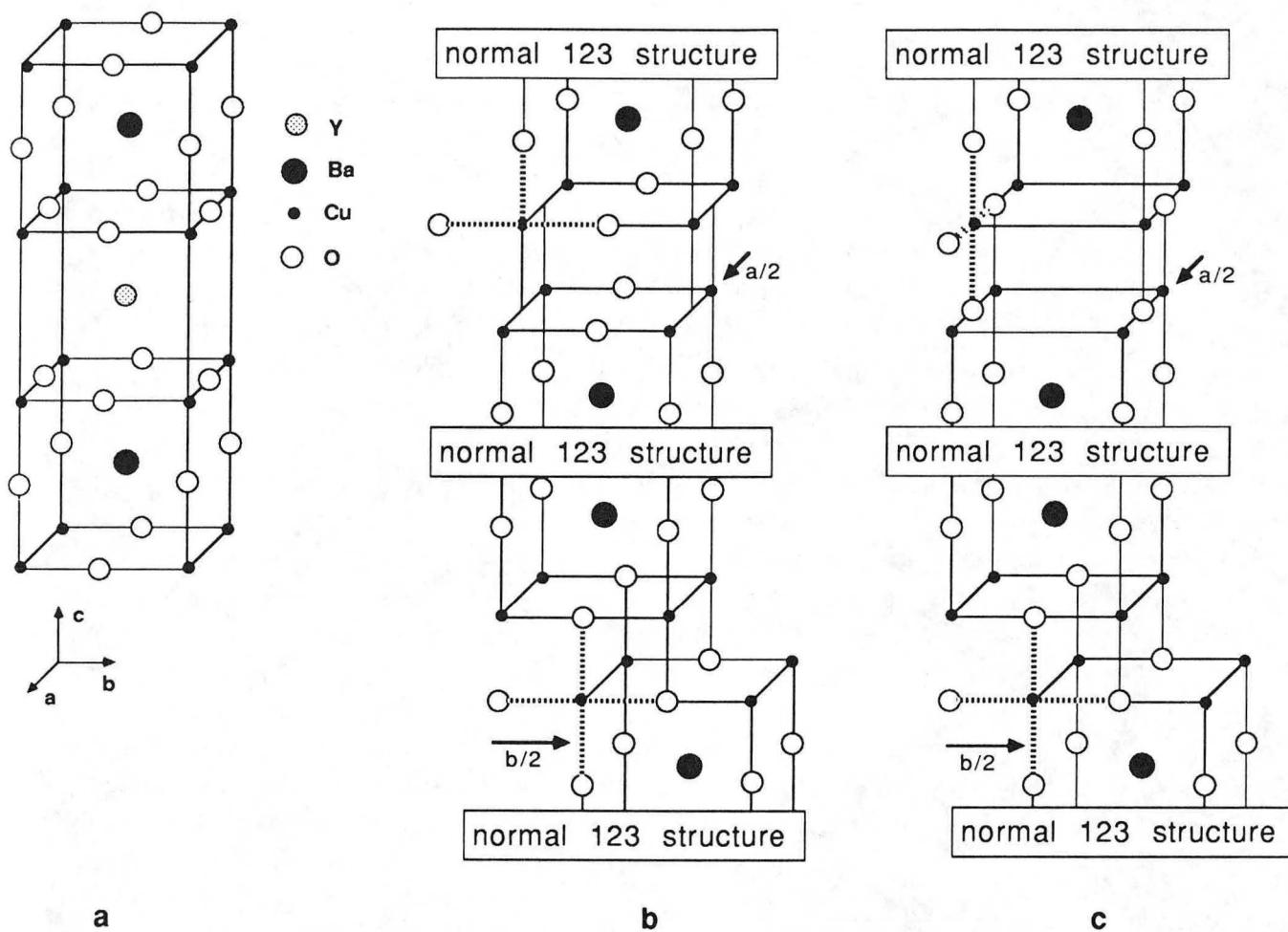
Acknowledgements

This work is supported by the Director, Office of Energy Research, Office of Basic Energy Sciences, Division of Materials Sciences, U.S. Department of Energy under Contract No. DE-AC03-76SF00098. The technical assistance of the staff of the National Center for Electron Microscopy is gratefully acknowledged.

References

1. J.G. Bednorz and K.A. Müller, *Z. Phys.* **B64**, 189 (1986).
2. J.D. Jorgensen, H.-B. Schuttler, D.G. Hinks, D.W. Capone II, K. Zhang, M.B. Brodsky, and D.J. Scalapino, *Phys. Rev. Lett.* **58**, 1024 (1987).
3. M.K. Wu, J.R. Ashburn, C.J. Torng, P.H. Hor, R.L. Meng, L. Gao, Z.J. Huang, Y.Q. Wang, and C.W. Chu, *Phys. Rev. Lett.* **58**, 908 (1987).
4. P.M. Grant, R.B. Beyers, E.M. Engler, G. Lim, S.S.P. Parkin, M.L. Ramirez, V.Y. Lee, A. Nazzari, J.E. Vasquez, and R.J. Savoy, *Phys. Rev. B* **35**, 7242 (1987).
5. Several reports are appropriate here:
 - J.M. Tarascon, L.H. Greene, W.R. McKinnon, and G.W. Hull, *Phys. Rev.* **B35**, 7115 (1987).
 - R.M. Hazen, L.W. Finger, R.J. Angel, C.T. Prewitt, N.L. Ross, H.K. Mao, and C.G. Hadjidiacos, *Phys. Rev.* **B35**, 7238 (1987).
 - T. Siegrist, S. Sunshine, D.W. Murphy, R.J. Cava, and S.M. Zahurak, *Phys. Rev.*, **B35**, 7137 (1987).
 - D.E. Cox, A.R. Moodenbaugh, J.J. Hurst, and R.H. Jones, *J. Phys. Chem. Solids*, (in press).
6. M.F. Garbaskas, R.H. Arendt, and J. S. Kasper, *Inorg. Chem.* **26**, 3191 (1987).
7. H.W. Zandbergen, G. van Tendeloo, T. Okabe, and S. Amelinckx, *phys. stat. sol.(a)* **103**, 45 (1987).
8. S. Takeda and S. Hikami, *Jpn. J. Appl. Phys.* **26** (1987) L848.
9. R. Beyers, G. Lim, E.M. Engler, R.J. Savoy, T.M. Shaw, T.R. Dinger, W.J. Gallagher, and R.L. Sandstrom *Appl. Phys. Lett.* **50**, 1918 (1987).
10. A. Ourmazd, J.A. Rentschler, J.C.H. Spence, M. O'Keefe, R.J. Graham, D.W. Johnson,

- Jr., and W.W. Rhodes, *Nature*, (1987) in press .
11. L.D. Marks, D. Tsurata, J. Theil, and K. Poeppelmeier, in Proc. of the 45th Ann. Meeting of the Electron Microscopy Soc. of America G.W. Bailey, (Ed.), San Francisco Press (1987) p. 56.
 12. M.P.A. Viegers, D.M. de Leeuw, C.A.H.A. Mutsaers, H.C.A. Smoorenburg, J.H.T. Hengst, J.W.C. de Vries and P.C. Zalm, to be published.
 13. H.W. Zandbergen, G.F. Holland, P. Tejedor, R. Gronsky, and A.M. Stacy, *Adv. Ceramic Mat.*, (1987) in press .
 14. B. Domenges, M. Hervieu, C. Michel, and B. Raveau, *Europhys. Lett.* **4** (2), pp 211-214 (1987).
 15. H.W. Zandbergen, R. Gronsky, M.Y. Chu, L.C. DeJonghe, G.F. Holland, and A.M. Stacy, MRS Proceedings, (1987), in press.
 16. H.W. Zandbergen, R. Gronsky, and G. Thomas, *phys. stat. sol.* **105**, 000 (1988).
 17. R. Gronsky and G. Thomas, in Proc. 41st Ann. Meeting Elec. Microscopy Soc. Amer., G.W. Bailey, (Ed.), Claitor's, Baton Rouge (1983) p. 310.
 18. R. Kilaas, in Proc. Microbeam Analysis Society (1987), in press.
 19. W.O. Saxton, *Inst. Phys. Conf. Ser.* **44**, Inst. of Phys., London (1978).
 20. C.C. Torardi, E.M. McCarron, M.A. Subramanian, H.S. Horowitz, J.B. Michel, A.W. Sleight, and D.E. Cox, *ACS Symposium Series*, Vol. **357** (1987).



XBL 881-23

Fig 1 The structure of perfect $\text{YBa}_2\text{Cu}_3\text{O}_7$ (a) and the defect layers for two different configurations (b) and (c), used in image calculations. Note that the shift along the a axis is accompanied by a rearrangement of the oxygen atoms in (c).

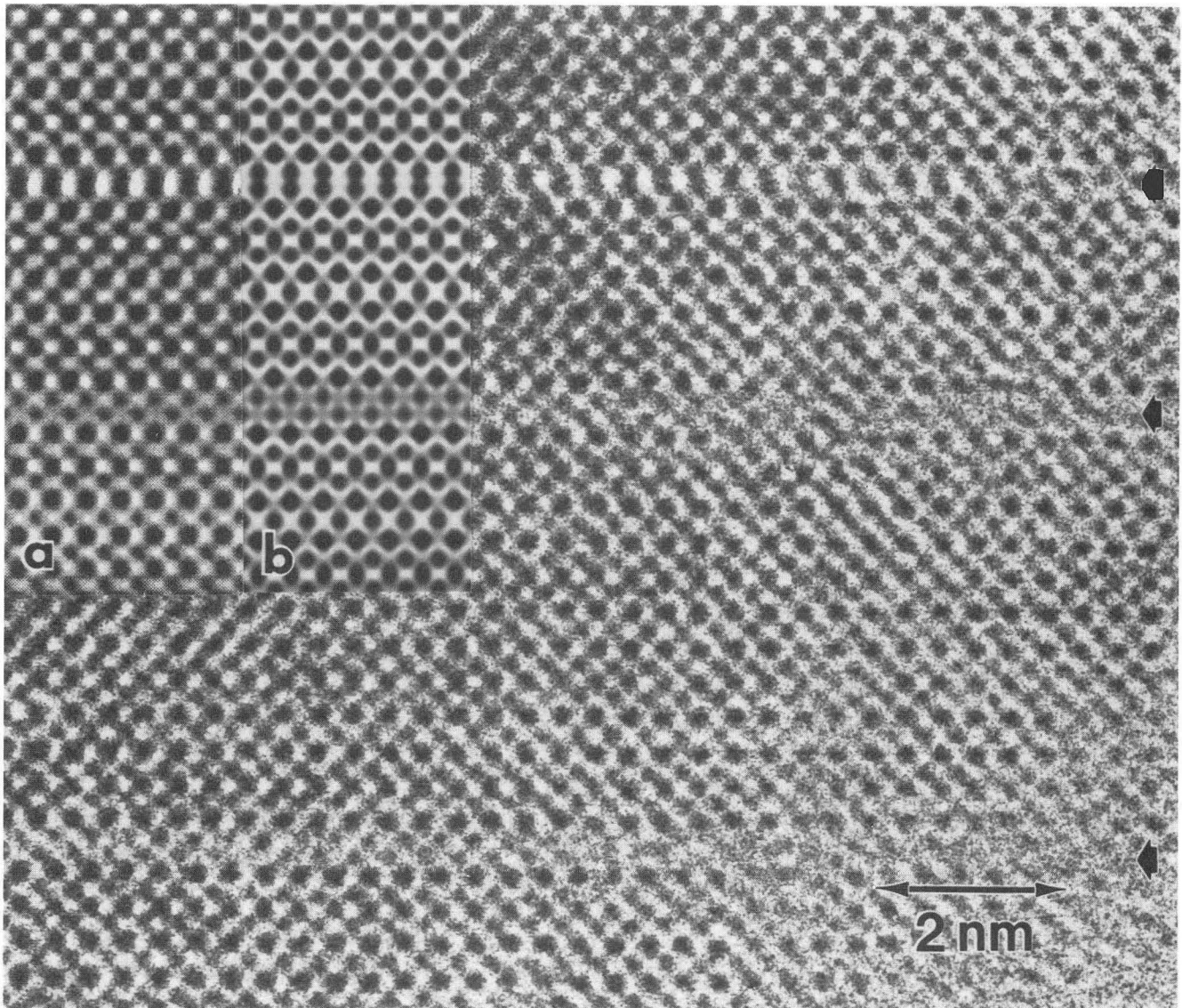
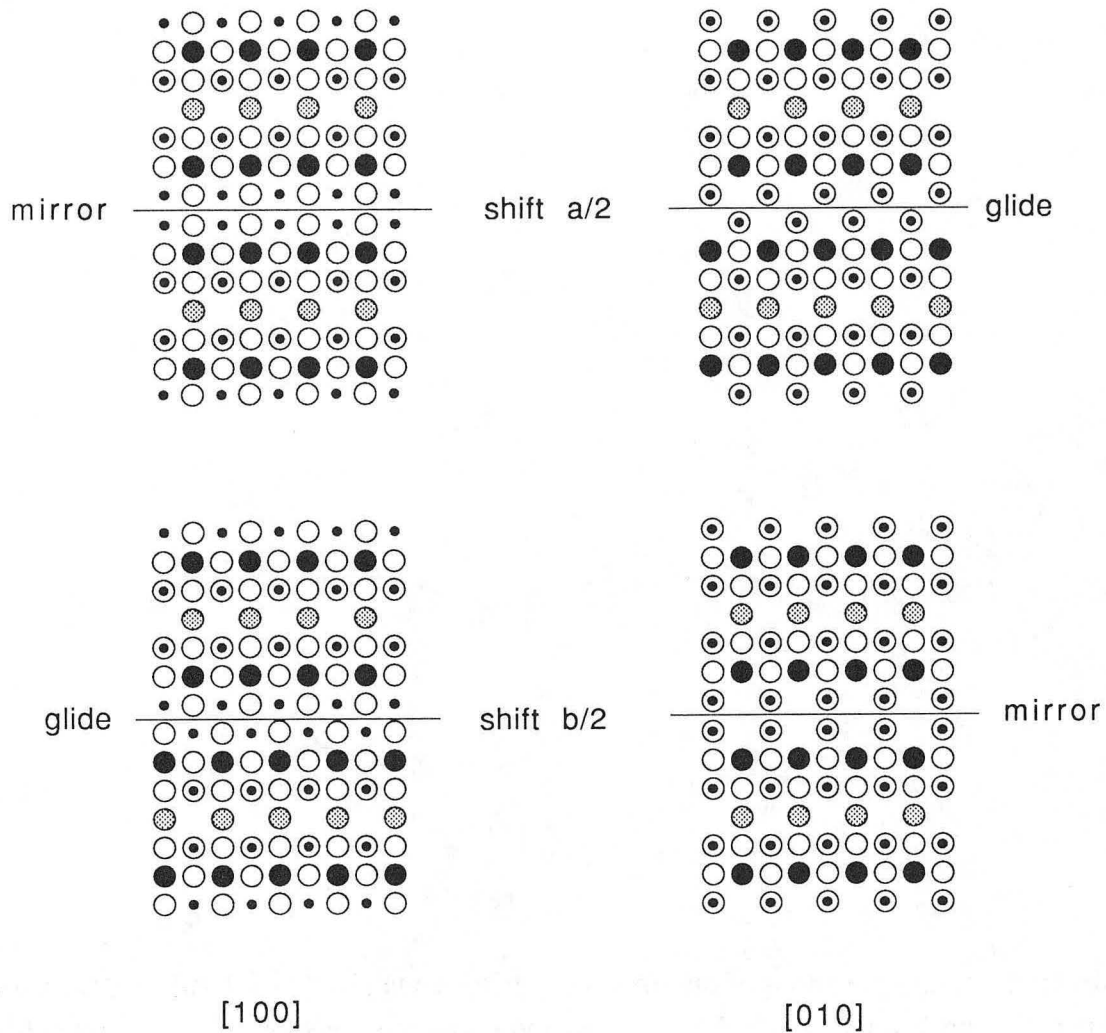


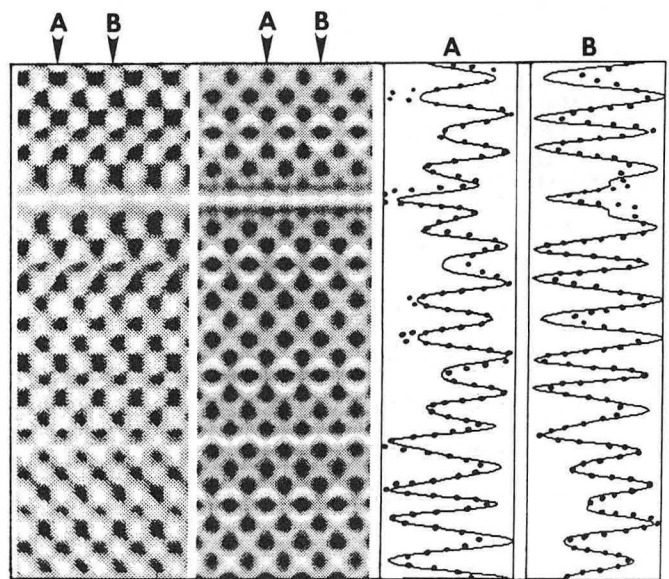
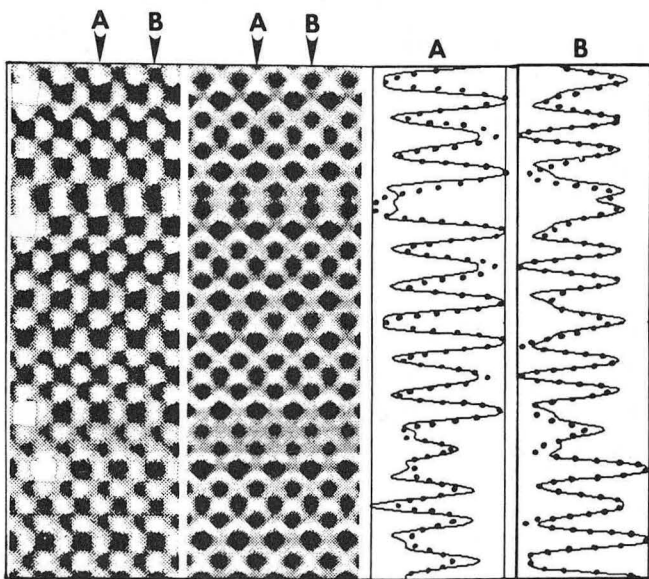
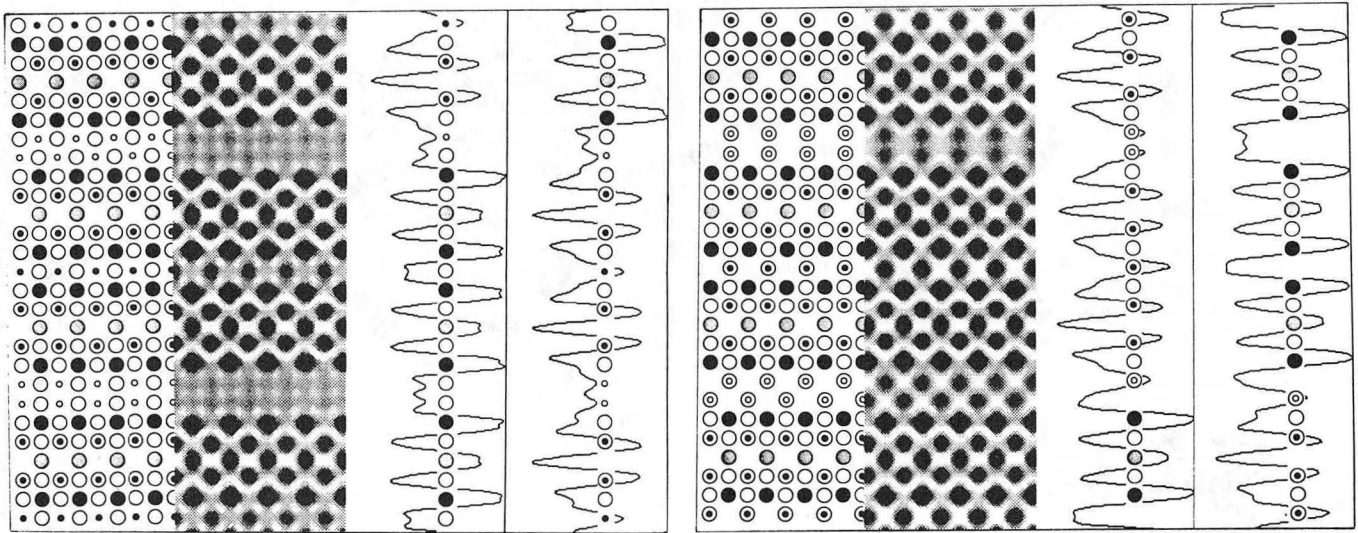
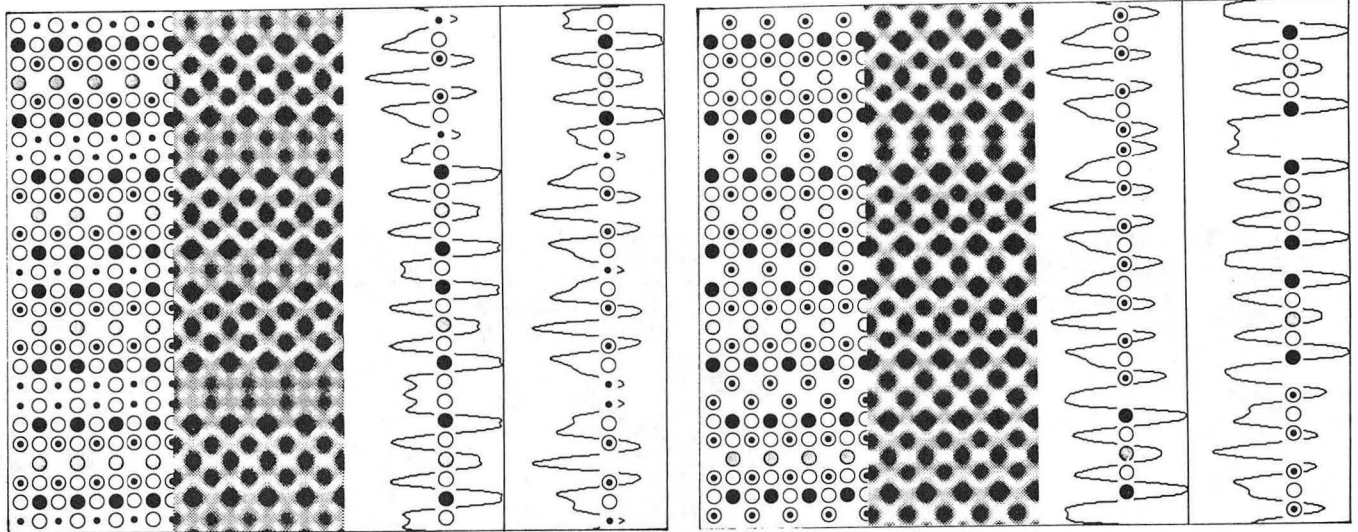
Fig 2 HREM image of $\text{YBa}_2\text{Cu}_3\text{O}_7$ in $[010]$ orientation showing defects (indicated by arrows) formed at room temperature. Two different defect images can be seen. The upper defect shows mirror symmetry and the other two, glide symmetry. Note that the upper defect gradually assumes glide character near the edge, suggesting that the length of the a axis is different on both sides of the defect. An averaged experimental image (a) and a calculated image (b) are inset. (XBB 8712-10598)



XBL 8712-5388

Fig 3 Structure models showing the resulting projected images with a shift of $a/2$ and $b/2$. A shift of $a/2$ leads to a defect layer with mirror symmetry when projected along $[100]$ and glide symmetry when projected along $[010]$. For a $b/2$ shift, the symmetries are reversed. The key for atomic representation is the same as in Figure 1. (XBL 8712-5388)

Fig 4 Two different interpretations of the structure viewed along $[100]$ and $[010]$. A projection of the structure model, a calculated image, and line scans are shown in (a) through (d). Full small circles represent fully-occupied Cu positions and open small circles represent half-occupied Cu positions. The locations at which the scans were made are indicated by the schematic row of atoms on which they are superimposed, where the thickness of a scanned line was 0.075 nm. The averaged experimental and calculated images at two different defocus values are shown in (e) and (f). Full lines represent calculated data, dotted lines the observed intensity variations in the images. The parameters used in the calculations are: specimen thickness, 2 nm; objective aperture, 6 nm^{-1} ; acceleration voltage, 1000 kV; spherical aberration coefficient, 2.8 mm; beam divergence angle, 0.6 mrad.(XBL 8712-5391)



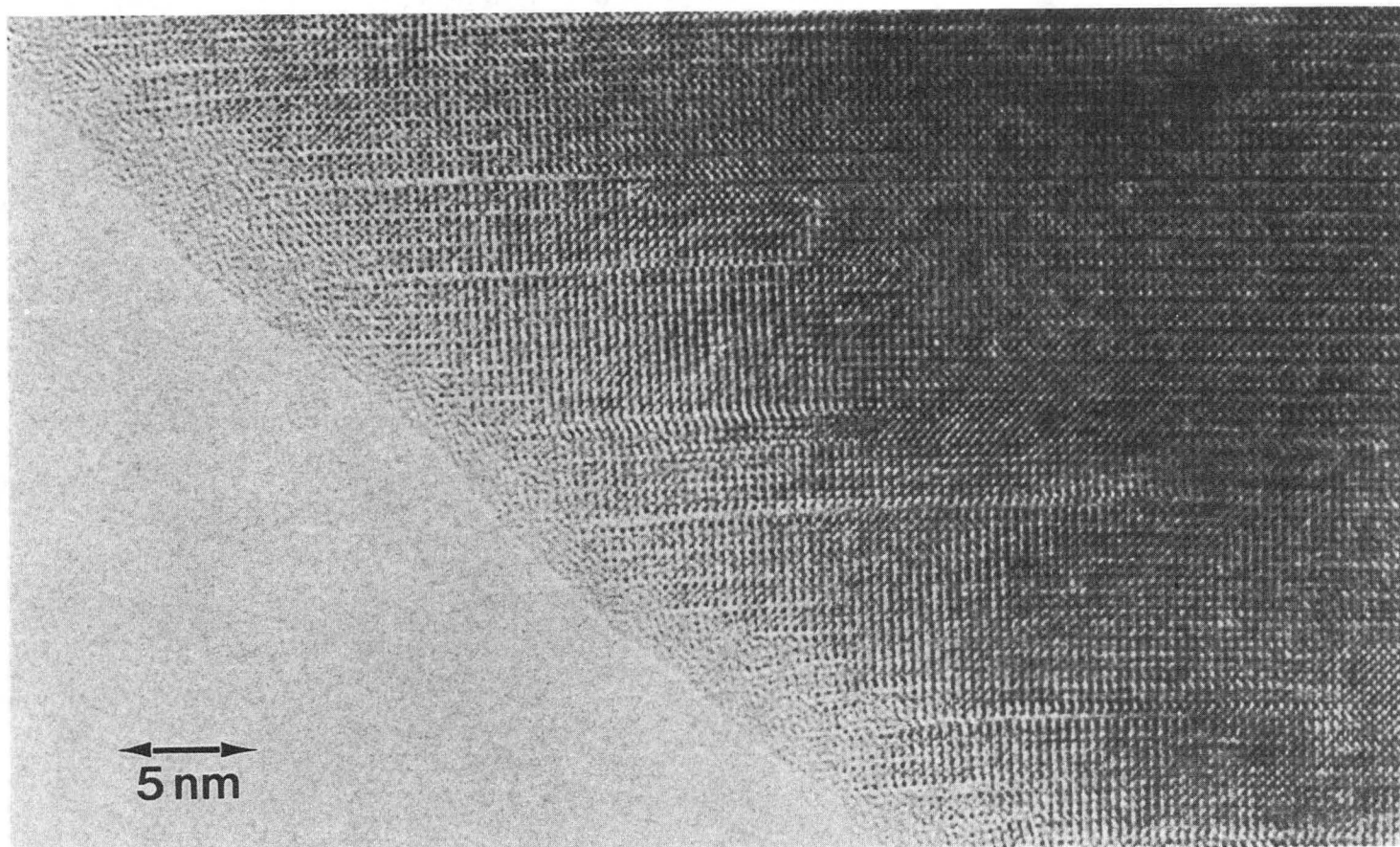


Fig 5 HREM image of the edge of a crystal in $[100]$ or $[010]$ orientation showing that the insertion of the CuO planes leads to a bending of the lattice. Often this insertion event is observed to occur in pairs. Due to a difference in the amount of bending along the electron beam direction between the surface layers and the interior layers, the symmetry of the image is locally reduced. (XBB 8712-10600)

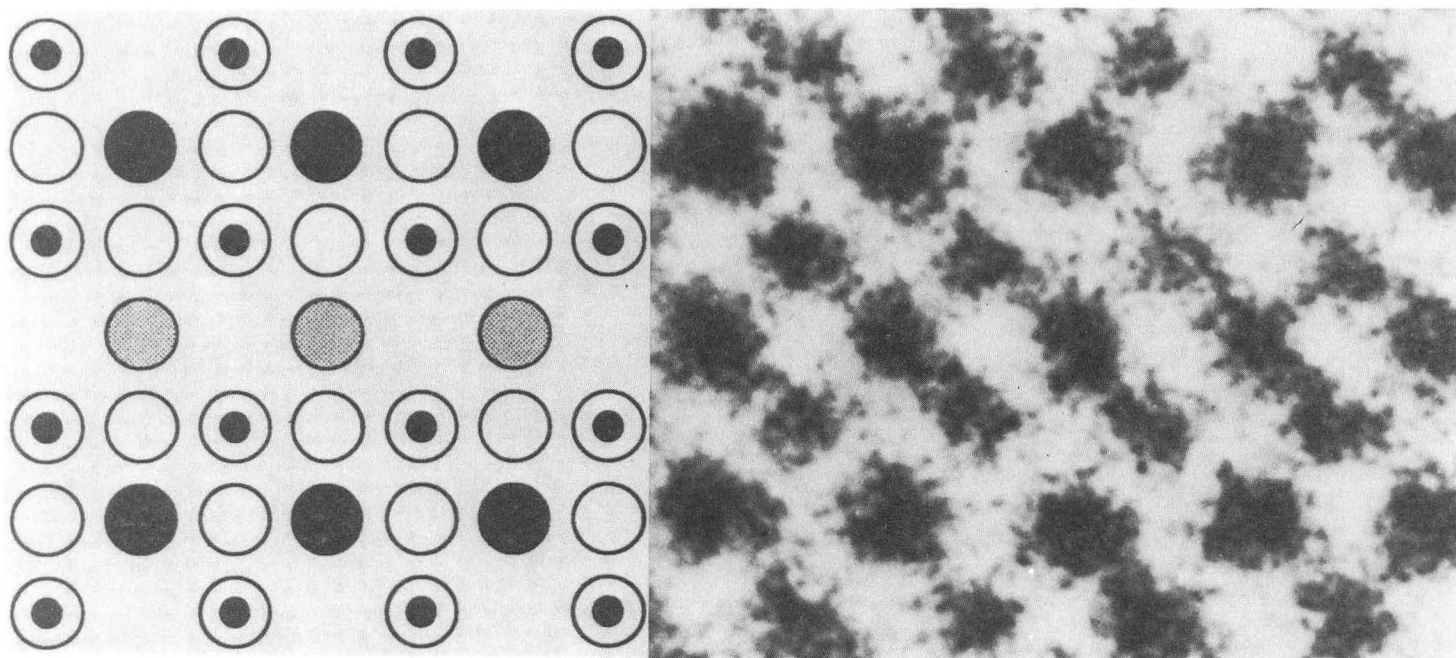


Fig 6 HREM image of $\text{YBa}_2\text{Cu}_3\text{O}_7$ in [010] orientation. The columns of Ba, Y and Cu are seen as separate black dots; atoms in the model are labeled as in Figure 1. (XBB 8712-10605)

*LAWRENCE BERKELEY LABORATORY
TECHNICAL INFORMATION DEPARTMENT
UNIVERSITY OF CALIFORNIA
BERKELEY, CALIFORNIA 94720*